Continuous Gas Phase Catalytic Transformation of Levulinic Acid to -Valerolactone over Supported Au Catalysts

Continuous Gas Phase Catalytic Transformation of Levulinic Acid to γ-Valerolactone over Supported Au Catalysts

Kamil Mustafin, Fernando Cárdenas-Lizana* and Mark A. Keane

Chemical Engineering, School of Engineering and Physical Sciences, Heriot-Watt University, Edinburgh EH14 4AS, Scotland

*corresponding author:

tel.: +44 (0) 131 451 4115, *e*-mail: F.CárdenasLizana@hw.ac.uk

ABSTRACT

BACKGROUND: γ-Valerolactone (GVL) is a high value chemical obtained from hydrogenation of bio-derived levulinic acid (LA). Work to date has focused on batch pressurised catalytic systems where high GVL yield is challenging. In this work, we examine the role of support redox and acidity properties in the continuous gas phase hydrogenation of aqueous LA at ambient pressure over gold on Al_2O_3, CeO_2 and TiO_2; Pd/Al_2O_3 served as a benchmark in catalyst tests.

RESULTS: We achieved 100% GVL yield under stoichiometric conditions (inlet H_2/LA = 1) over supported Au (mean size = 3.0-4.3 nm). Greater catalytic activity was recorded for Au on reducible TiO_2 and CeO_2. Under the same reaction conditions, Pd/Al_2O_3 delivered higher LA consumption rates but promoted formation of pentanoic acid.

CONCLUSIONS: GVL formation proceeds *via* 4-hydroxypentanoic as reactive intermediate. Surface oxygen vacancies (confirmed by O_2 titration) formed during temperature programmed reduction of reducible oxides activate LA for reaction. Greater GVL productivity (with full hydrogen utilisation) is demonstrated in this work relative to state-of-the art supported Pd and Ru catalysts.

Keywords*:* Selective hydrogenation; levulinic acid; γ-valerolactone; Au catalysts; support effects.

1 SYMBOLS

LA	Levulinic acid
GVL	γ-Valerolactone
HPA	Hydroxypentanoic acid
AGL	α-Angelica lactone
i.d.	Internal diameter, mm
d	Metal nanoparticle mean size, nm
TPR	Temperature programmed reduction
TPD	Temperature programmed desorption
TCD	Thermal conductivity detector
SSA	Specific surface area, $m^2\ g^{-1}$
STEM	Scanning transmission electron microscopy
T_{max}	Temperature maximum in catalyst activation by TPR, K
P	Pressure, atm
T	Reaction temperature, K
L_{bed}	Catalyst bed length, mm
V_{bed}	Catalyst bed volume, mm^3
n	Moles of metal in the catalyst bed, mol
F	Levulinic acid feed rate, mol h^{-1}
GHSV	Gas hourly space velocity, h^{-1}
FID	Flame ionisation detector
X	Fractional conversion
S_j	Selectivity to product "j", %
k	Kinetic rate constant, h^{-1}

INTRODUCTION

γ-Valerolactone (GVL) is a lignocellulose building block chemical used as an intermediate in alkane (jet fuel, gasoline and diesel fuel), aromatic (fuel additives), polymer and solvent production.[1] The main route to GVL is the hydrogenation of levulinic acid (LA), obtained from cellulose, starch, or C6 sugars[2] *via* low cost ($0.09-0.22 kg^{-1}) acid hydrolysis.[3,4] The reaction pathways from a compilation of the literature[5-7] on LA → GVL transformation are presented in **Figure 1**. GVL production proceeds *via* hydrogenation and dehydration steps. The predominant pathway is still a matter of debate where variations in operating conditions,[5] choice of support[8] and metal[9] or solvent[10] impacts on catalytic activity and/or selectivity.

The catalytic hydrogenation of LA using both homogeneous[11] and heterogeneous[5] systems has been investigated. Heterogeneous catalysis offers advantages in terms of product separation and catalyst reuse. Work to date has largely dealt with pressurised (5-250 bar) batch liquid phase conversion in organic solvents (1,4-dioxane, methanol and toluene) where full selectivity to GVL at high conversions remains challenging.[11-14] Continuous GVL formation at ambient pressure facilitates higher throughput. In catalytic hydrogenation, control over contact time can govern conversion[15] and selectivity.[16] Reviews by Wright and Palkovits in 2012,[5] Yan *et al.* in 2015[7] and Delidovich *et al.* in 2016[17] identified supported Pd and Ru as the best catalysts for continuous gas phase transformation of LA with a productivity of 81-91 $mmol_{GVL}\ g_{metal}^{-1}\ h^{-1}$ and 90-98.6% GVL yield. Use of toxic 1,4-dioxane[18] as solvent and excess hydrogen are process sustainability issues to be addressed.

The use of supported gold catalysts for the transformation of biomass-derived feedstock to value-added chemicals is showing promise.[19] Notable examples include aldehyde reduction (*e.g.* 2-hydroxymethyl-5-furfural → 2,5-bis(hydroxymethyl)furan)[20],

dehydration of carbohydrates[21] and hydrogenation/dehydration of succinic anhydride to γ-butyrolactone[22]. Lewis and Brønsted acid sites contribute to catalytic dehydration[23] (**Figure 1**, steps **(I)**, **(IV)**, **(VII)**, and **(VIII)**). In the case of reducible oxide supports (*e.g.* titania and ceria), oxygen vacancies generated by the loss of structural oxygen from the oxide sub-lattice[24] can modify reactant adsorption/activation and influence catalytic performance[25]. These vacancies can fix oxygen in water,[26] alcohols[27] and aldehydes[28]. Increased rate and carbonyl reduction selectivity in the conversion of aldehydes has been ascribed to facilitated -C=O activation at oxygen deficient sites in CeO_2[29] and Fe_2O_3[30]. Using DFT calculations, Baker *et al.*[31] identified oxygen vacancies in Pd/TiO_2 as the catalytically active sites for -C=O reduction in furfural hydrogenation. The opposite effect is also possible where strong binding of oxygenated reactants to these vacancies[32] has been deemed responsible for lower hydrogenation activity.[33]

In this work, we evaluate the impact of the support redox (reducibility) and acid properties in the continuous hydrogenation of LA over a series of oxide (Al_2O_3, CeO_2 and TiO_2) supported Au catalysts, taking Pd/Al_2O_3 as a benchmark. We examine the reaction pathways and consider the effect of varying inlet H_2/LA, using water as a solvent with a view to clean production of GVL.

EXPERIMENTAL

Catalyst Preparation and Activation

The oxide carriers (γ-Al_2O_3 (Puralox, Condea Vista Co.), CeO_2 (Grace Davison) and TiO_2 (P25, Degussa)) were used as received. Supported (1.0-3.0% wt.) Au catalysts were prepared by deposition-precipitation. Urea (100-fold excess, Riedel-de Haën, 99%), used as basification agent, was added to an aqueous solution of $HAuCl_4$ ($4 \times 10^{-5} - 5 \times 10^{-3}$ M; 20–50 cm^3, Sigma-Aldrich，99%) containing the support (5-30 g). The suspension was stirred and

heated to 353 K (2 K min^{-1}) for 3 h in a He purge where the pH progressively increased to *ca.* 7 after 3 h as a result of thermally induced urea decomposition with Au^{3+} deposition.[34] The resultant solid was separated by centrifugation, washed with deionised water until the wash water was Cl-free ($AgNO_3$ test) and dried in He (45 cm^3 min^{-1}) at 373 K (2 K min^{-1}) for 5 h. A commercial Pd/Al_2O_3 (1.2% wt. Pd, Sigma-Aldrich) catalyst was employed as benchmark. Prior to use, the catalysts were sieved to 75 μm average particle diameter (ATM fine test sieves) and activated in 60 cm^3 min^{-1} H_2 at 2 K min^{-1} to 573–603 K. Samples were passivated in 1% v/v O_2/He at ambient temperature for *ex situ* analysis.

Catalyst Characterisation

The (Au and Pd) metal content was measured by atomic absorption spectroscopy (Shimadzu AA-6650 spectrometer with an air-acetylene flame) from the diluted extract in aqua regia (25% v/v HNO_3/HCl). Temperature programmed reduction (TPR), $H_2/O_2/NH_3$ chemisorption, temperature programmed desorption (TPD) and specific surface area (SSA) measurements were recorded using the commercial CHEM-BET 3000 (Quantachrome Instruments) unit equipped with a thermal conductivity detector (TCD) for monitoring gas composition and the TPR Win™ software for data acquisition/manipulation. Samples (0.05-0.1 g) were loaded into a U-shaped Quartz cell (3.76 mm i.d.), outgassed for 30 min and total SSA recorded in a 30% v/v N_2/He flow with undiluted N_2 (BOC, 99.9%) as internal standard. Two cycles of N_2 adsorption-desorption were employed using the standard single point BET method. TPR analysis was conducted in 17 cm^3 min^{-1} (Brooks mass flow controller) 5% v/v H_2/N_2 at 2 K min^{-1} to 573–603 K where the effluent gas passed through a liquid N_2 trap. Samples were maintained at the final isothermal hold in a flow of H_2/N_2 until the signal returned to baseline, swept with 65 cm^3 min^{-1} N_2 for 1.5 h, cooled to reaction (493 K, H_2 chemisorption) or ambient (NH_3 chemisorption) temperature and subjected to pulse (10-1000

µl) titration (BOC, ≥99.98%). Hydrogen/ammonia pulses were repeated until the signal area was constant and there was no detectable uptake. Ammonia TPD was conducted to determine total acidity.[35] Samples were thoroughly flushed in N_2 (65 cm^3 min^{-1}) for 1.5 h post-NH_3 titration to remove weakly bound NH_3 and heated at 30 K min^{-1} (in 65 cm^3 min^{-1} N_2) to 973 K. Oxygen chemisorption was performed to assess the extent of support reduction,[36] where the samples were swept with 65 cm^3 min^{-1} He for 1.5 h post-TPR, cooled to 493 K and subjected to O_2 pulse (10 µl) titration. It has been demonstrated elsewhere that Au contribution to total O_2 adsorbed is negligible.[37] SSA and gas uptake values were reproducible to ±5%. Gold and Pd metal particle morphology (size and shape) was determined by scanning transmission electron microscopy (STEM) using a JEOL 2200FS operated at an accelerating voltage of 200 kV, employing Gatan Digital Micrograph 1.82 for data acquisition/manipulation. Samples for analysis were prepared by dispersion in acetone and deposited on a holey Cu grid (300 mesh). The number weighted mean Au and Pd diameters (*d*) were determined from a count of up to 800 particles.[38]

Gas Phase Hydrogenation of Levulinic acid (LA)

Materials

LA (98%) and GVL (99%) were supplied by Sigma-Aldrich and used as received. All the gases (H_2, N_2, O_2 and He) were of ultra-high purity (BOC, ≥99.99%).

Catalytic System

Reactions were performed at ambient pressure over the temperature range 493-573 K, immediately after *in situ* catalyst activation in a fixed bed vertical continuous plug-flow glass reactor (i.d. = 12 mm). A layer of borosilicate glass balls (2 mm diameter; height = 3 cm) served as preheating zone, ensuring the reactant was vaporised and reached reaction

temperature before contacting the catalyst. Isothermal conditions (±1 K) were maintained by diluting the catalyst bed (L_{bed} = 2 mm; V_{bed} = 226 mm^3; fraction of catalyst in the bed by volume = 0.1-1) with ground glass (75 μm). Reaction temperature was continuously monitored by a thermocouple inserted in a thermowell within the catalyst bed. An aqueous or organic (toluene) solution of LA (0.29 M) was delivered to the reactor *via* a glass/teflon air-tight syringe and a teflon line at a fixed calibrated flow rate using a microprocessor controlled infusion pump (Model 100, KD Scientific). A co-current flow of LA and H_2, N_2 or H_2+N_2 was maintained at $GHSV = 2 \times 10^4$ h^{-1} where inlet H_2/LA was varied from stoichiometry (=1 for GVL formation) to far in excess (=420); gas flow rate was monitored using a Humonics (Model 520) digital flowmeter. The molar metal (n) to inlet LA feed rate (F) spanned the range $5 \times 10^{-4} - 1 \times 10^{-2}$ h. In a series of blank tests, reactions using GVL or LA as reactant in a stream of H_2 through the empty reactor or over the support alone did not result in any detectable conversion.

Analytical Method and Activity/Selectivity Evaluation

The reactor effluent was frozen in a liquid nitrogen trap and analysed by capillary GC (Perkin-Elmer Auto System XL gas chromatograph equipped with a programmed split/splitless injector and flame ionisation detector (FID)) using a Stabilwax (fused silica) 30 m × 0.32 mm i.d., 0.25 μm film thickness capillary column (RESTEK), employing Turbo-Chrom Workstation Version 6.3.2 (for Windows) for data storage and manipulation. Product composition was based on detailed calibration plots (not shown) using commercial samples. Catalytic activity is quantified in terms of fractional conversion (X)

$$X = \frac{LA_{in} - LA_{out}}{LA_{in}} \quad \textbf{(1)}$$

extracted from time on-stream measurements.[39] Selectivity in terms of the target GVL (S_{GVL})

is given by

$$S_{GVL} = \frac{GVL_{out}}{LA_{in} - LA_{out}} \times 100 \quad \textbf{(2)}$$

where the subscripts "in" and "out" refer to the inlet and outlet streams. Repeated reactions with different samples from the same batch of catalyst delivered conversion/selectivity values reproducible to within ±5%; carbon mass balance was complete to better than ±9%.

RESULTS AND DISCUSSION

Catalyst Characterisation

Catalyst physico-chemical characteristics are given in **Table 1**. The SSA range from 52 $m^2\ g^{-1}$ (Au/TiO_2) to 166 $m^2\ g^{-1}$ (Au/Al_2O_3) and the values obtained for each system are in agreement with those reported in the literature.[40,41] The TPR profiles of laboratory synthesised Au/Al_2O_3 **(A)**, Au/CeO_2 **(B)** and Au/TiO_2 **(C)** are presented in **Figure 2(I)** with associated H_2 consumption in **Table 1**. Activation of Pd/Al_2O_3 by TPR followed the procedure described previously.[42] Au/Al_2O_3 exhibited a single positive peak at 461 K that is comparable with the literature.[43] Hydrogen consumption matched the requirements for $Au^{3+} \rightarrow Au^0$. A lower temperature reduction peak was in evidence for Au/CeO_2 (T_{max} = 420 K) and Au/TiO_2 (T_{max} = 376 K) and can be linked to weaker Au-support interactions[40] resulting in a more facile reduction of the metal phase[44]. Hydrogen consumption during TPR of Au/CeO_2 (5×10^2 μmol g^{-1}) and Au/TiO_2 (2×10^2 μmol g^{-1}) exceeded the amount required for reduction of the metal precursor (**Table 1**), indicative of partial support reduction.[45] Hydrogen chemisorption on all the Au catalysts was lower than the benchmark Pd/Al_2O_3 (**Table 1**), which can be explained by the higher activation barrier for dissociative H_2 adsorption on Au.[46] The consensus from the literature suggests that H_2 adsorption on Au is dependent on temperature and Au coordination.[47] Smaller Au particles exhibit a greater

preponderance of corner and edge sites that facilitate H_2 adsorption, which is favoured by a higher titration temperature.[48] Dissociated H_2 chemisorbed on Au can spill onto the support and promote superficial reduction of the oxide carrier with the generation of oxygen vacancies, an effect that has been reported for Au/CeO_2[49] and Au/TiO_2[50].

Oxygen chemisorption post-TPR was negligible on Au/Al_2O_3 and Pd/Al_2O_3 (**Table 1**), consistent with the *non*-reducibility of Al_2O_3 where temperatures ≥1373 K are required for oxide reduction.[51] Greater uptake on Au/CeO_2 and Au/TiO_2 is consistent with vacancy formation during TPR of these reducible oxides. Representative STEM images **(I)** and associated particle size distribution histograms **(II)** for Au/Al_2O_3 **(A)**, Au/CeO_2 **(B)** and Au/TiO_2 **(C)** are provided in **Figure 3**. The Au particles are in the 1-8 nm size range, which has been identified as crucial for hydrogenation activity.[52] Au/CeO_2 and Au/TiO_2 showed a narrower distribution of smaller metal particles, which can be linked to stabilisation at oxygen vacancies that serves to inhibit sintering during TPR.[53] The Pd/Al_2O_3 sample exhibited similar mean metal size (**Table 1**) and is a suitable reference catalyst to assess the catalytic performance of supported Au in LA hydrogenation.

Surface acidity was determined by NH_3 chemisorption/TPD. Total acidity measurements coincided for titration and TPD; the desorption profiles for Au/Al_2O_3 **(A)**, Au/CeO_2 **(B)** and Au/TiO_2 **(C)** are provided in **Figure 2(II)**. The three catalysts exhibited a principal desorption peak for NH_3 release over the 600-973 K range, characteristic of strong acid sites, *i.e.* NH_3 desorption at $T \geq 673$ K.[8,54] Surface acidity in the case of Al_2O_3, CeO_2 and TiO_2 is associated with uptake at Al^{3+}, Ce^{4+} or Ti^{4+} Lewis acid centres, as demonstrated by XPS,[55] temperature-programmed reaction,[55] NMR[56] and FT-IR[57,58] measurements. The quantity of NH_3 chemisorbed/desorbed (**Table 1**) on the three Au catalysts (12-28 × 10^{-2} mmol g^{-1}) was comparable with that reported for Al_2O_3,[40,41] CeO_2,[59] and TiO_2[60,61] supported Au systems (10-

38×10^{-2} mmol g^{-1}).

Catalyst Performance

Reaction over supported Au under conditions of excess hydrogen (H_2/LA = 420) generated GVL as sole product at $X \leq 0.75$ (**Figure 4(I)**). This response finds agreement with the work of Du *et al.*[62] in batch liquid phase conversion of LA + formic acid (5 bar) over (ZrO_2, TiO_2, SiO_2) supported Au where CO_2 was formed as by-product (from formic acid). We provide here the first reported catalytic data for gas phase continuous flow operation at ambient pressure over Au catalysts. Taking the reaction pathways presented in **Figure 1**, GVL generation through the formation of (levulinic and hydroxy levulinic) esters (steps **(I-II)**) is associated with batch liquid operation with alcohol solvents.[63] The LA → GVL composite hydrogenation/dehydration is possible *via* two routes. Reaction through steps **(VI)** and **(VII)** involves hydrogenation of the ketone group at metal sites to form 4-hydroxypentanoic acid (HPA) that undergoes acid-catalysed ring closure (intramolecular esterification).[6] There is theoretical (DFT)[64,65] and experimental[65] evidence that LA → HPA hydrogenation (step **(VI)**) is rate-determining. HPA is highly reactive and readily undergoes dehydration to GVL.[66] Alternatively, dehydration of LA (step **(VIII)**) on acid sites generates α-angelica lactone (AGL) that undergoes reduction to GVL (step **(IX)**).[67] The HPA or AGL intermediates were not isolated in the product mixture. Conversion of LA to AGL *via* step **(VIII)** is favoured by replacing H_2 with N_2 as gas carrier, circumventing reduction (step **(VI)**). Switching from H_2O to toluene as LA solvent should also favour dehydration to AGL. Reaction (at 573 K) in N_2 using toluene over the three Au catalysts resulted in exclusive LA → AGL at a similar low conversion ($X \leq 0.08$). At the same reaction temperature, catalyst tests using the three systems in H_2 with H_2O promoted LA → GVL at 10-fold higher conversion. Transformation of an aqueous LA feed (in H_2) to GVL must proceed

predominantly *via* HPA in a sequential hydrogenation and dehydration (steps **(VI)** and **(VII))**. It is established that acid sites contribute to dehydration.[23] The three Au catalysts exhibit similar surface acidity (see **Figure 2(II)** and **Table 1**), which did not promote significant LA → AGL but must contribute to HPA → GVL (step **(VII)**) in the sequential conversion of LA. Balla *et al.*[68] and Kumar and co-workers[69] showed that catalytic activity in the gas phase transformation of LA → AGL is dependent on the concentration[68] and type[69] of acid sites.

We have previously established the applicability of pseudo-first order kinetics for hydrogenation over Au under plug-flow conditions where H_2 was maintained in excess[47] according to

$$\ln(1-X)^{-1} = k \times \left(\frac{n}{F}\right) \qquad \textbf{(3)}$$

where the parameter *n/F* has the physical significance of contact time. The rate constants (*k*) obtained from linear regression of $\ln(1-X)^{-1}$ *vs*. *n/F* (**Figure 5**) were fitted to an Arrhenius expression to give an apparent activation energy for LA → GVL of 35 kJ mol^{-1} (see inset to **Figure 5** for Au/Al_2O_3). This is within the range (26-54 kJ mol^{-1})[6] reported for liquid phase reaction over Ru catalysts. The activity of Au/Al_2O_3 was appreciably lower than that of Au on reducible supports (**Table 1**). Differences in rate can result from variations in H_2 uptake under reaction conditions.[70] However, the three supported catalysts exhibit an equivalent chemisorption capacity (**Table 1**). It is significant that Au/CeO_2 and Au/TiO_2 with similar density of oxygen vacancies (and greater than Au/Al_2O_3) delivered an equivalent catalytic activity. A possible contribution due to LA adsorption/activation at these vacancies should then be considered. Calaza *et al.*[71] have established (by TPD, RAIRS and DFT) carbonyl group activation at oxygen vacancies on CeO_2. To probe this effect we evaluated the catalytic response of physical mixtures of Au/Al_2O_3 with (non-reducible) Al_2O_3 and (reducible)

TiO_2/CeO_2. Reaction over $Au/Al_2O_3+Al_2O_3$ and Au/Al_2O_3 delivered the same LA consumption rate (300 $mmol_{GVL}\ g_{metal}^{-1}\ h^{-1}$). In contrast, $Au/Al_2O_3+TiO_2$ and $Au/Al_2O_3+CeO_2$ combinations exhibited measurably higher rates (500-600 $mmol_{GVL}\ g_{metal}^{-1}\ h^{-1}$). Oxygen vacancy formation in CeO_2 and TiO_2 as part of the $Au/Al_2O_3+TiO_2$ and $Au/Al_2O_3+CeO_2$ mixtures is possible by spillover hydrogen migration across solid/solid grain boundaries.[72] The greater activity of Au/Al_2O_3 with reducible CeO_2 and TiO_2 suggests a direct contribution of these surface defects to catalytic activity. A similar conclusion was reached by Manyar *et al.*[73] and Hu and co-workers[74] in the hydrogenation of carboxylic acids and dimethyl succinate (to γ-butyrolactone) over TiO_2 supported Pt and Mn spinel-supported Cu, respectively. At higher LA conversion ($X > 0.75$), GVL selectivity declined (**Figure 4(I)**) due to the formation of pentanoic acid. The generation of pentanoic acid can result from HPA hydrogenation-dehydration (step **(IV)** in **Figure 1**) or further conversion of GVL (step **(V)**). Kumar *et al.*[69] has shown by combined pyridine adsorption/DRIFTS analysis and kinetic measurements that acid sites promote GVL ring opening to pentanoic acid. Using GVL as reactant under the same reaction conditions, we recorded negligible conversion ($X < 0.03$), suggesting step **(IV)** as the predominant source of pentanoic acid.

Unwanted transformation of HPA to pentanoic acid (*via* step **(IV)** in **Figure 1**) requires hydrogen. With a view to maximise GVL formation and limit pentanoic acid formation we evaluated the catalytic response to modifications in H_2 content in the feed (inlet H_2/LA); the results obtained are presented in **Figure 4(II)**. A decrease in H_2/LA served to increase GVL selectivity to reach 100% yield over the three catalysts under stoichiometric conditions. Levulinic acid transformation is typically operated under an excess of pressurised gaseous H_2 in order to maximise product yield.[11-13] Mohan *et al.*[75] studied the effect of H_2/LA molar ratio for reaction over Ni/H-ZSM-5 and reported a maximum 92% GVL yield at H_2/LA

= 8. The authors recorded lower conversions at H_2/LA < 8 while formation of pentanoic acid was promoted at H_2/LA > 8. To the best of our knowledge, this is the first report of 100% GVL yield in continuous operation with full hydrogen utilisation. Under these reaction conditions, Pd/Al_2O_3 delivered a higher LA consumption rate than Au/Al_2O_3 (1090 *vs.* 300 $mmol_{GVL}$ g_{metal}^{-1} h^{-1}), that correlates well with the reported higher activity for Pd (*vs.* Au) in hydrogenations[76,77] but promoted undesired pentanoic acid ($S_{Pentanoic\ acid}$ = 10%). We have recorded 100% yield of GVL with an order of magnitude greater productivity relative to the state-of-the art supported Pd and Ru catalysts[5,7,17]. Our results demonstrate that oxide supported Au promotes GVL formation *via* HPA where catalytic activity is sensitive to the redox nature of the oxide carrier.

CONCLUSIONS

In the gas phase continuous catalytic conversion of (aqueous) LA, 100% yield of target GVL was achieved under stoichiometric conditions (H_2/LA = 1) over oxide (Al_2O_3, CeO_2 and TiO_2) supported Au. The formation of GVL results from hydrogenation/dehydration with HPA as reactive intermediate. Oxygen titration following TPR established partial reduction of CeO_2 and TiO_2 where Au on reducible supports delivered a higher GVL production rate (relative to Au/Al_2O_3) that is linked to LA activation at surface oxygen vacancies. Palladium on Al_2O_3 as benchmark exhibited higher LA consumption rates but promoted formation of pentanoic acid. Higher H_2 feed content (H_2/LA >2) generated pentanoic acid over the Au catalysts. Continuous GVL formation at ambient pressure from an aqueous LA feed represents a significant advancement over current pressurised batch liquid operations using organic solvents. We have demonstrated full hydrogen utilisation and an order of magnitude higher GVL production rate than current state-of-the art supported Pd and Ru catalysts.

ACKNOWLEDGEMENTS

We thank Janis Eglitis for his contribution to this work.

REFERENCES

1. Alonso DM, Wettstein SG, Dumesic JA, Gamma-valerolactone, A Sustainable Platform Molecule Derived from Lignocellulosic Biomass. *Green Chem.* **15**: 584-595 (2013).
2. Girisuta B, Janssen LPBM, Heeres HJ, International Conference on Sustainable (Bio)Chemical Process Technology Green Chemicals. *Chem. Eng. Res. Des.* **84**: 339-349 (2006).
3. Weingarten R, Kim YT, Tompsett GA, Fernández A, Han KS, Hagaman EW, Conner.Jr. WC, Dumesic JA, Huber GW, Conversion of Glucose into Levulinic Acid with Solid Metal(IV) Phosphate Catalysts. *J. Catal.* **304**: 123-134 (2013).
4. Patel AD, Serrano-Ruiz JC, Dumesic JA, Anex RP, Techno-economic Analysis of 5-Nonanone Production from Levulinic Acid. *Chem. Eng. J.* **160**: 311-321 (2010).
5. Wright WRH and Palkovits R, Development of Heterogeneous Catalysts for the Conversion of Levulinic Acid to γ-Valerolactone. *ChemSusChem* **5**: 1657-1667 (2012).
6. Abdelrahman OA, Heyden A, Bond JQ, Analysis of Kinetics and Reaction Pathways in the Aqueous-phase Hydrogenation of Levulinic Acid to form γ-Valerolactone over Ru/C. *ACS Catal.* **4**: 1171-1181 (2014).
7. Yan K, Yang Y, Chai J, Lu Y, Catalytic Reactions of Gamma-valerolactone: A Platform to Fuels and Value-added Chemicals. *Appl. Catal. B: Environ.* **179**: 292-304 (2015).
8. Mohan V, Venkateshwarlu V, Pramod CV, Raju BD, Rao KSR, Vapour Phase Hydrocyclisation of Levulinic Acid to γ-Valerolactone over Supported Ni Catalysts. *Catal. Sci. Technol.* **4**: 1253-1259 (2014).
9. Upare PP, Lee J-M, Hwang DW, Halligudi SB, Hwang YK, Chang J-S, Selective Hydrogenation of Levulinic Acid to γ-Valerolactone over Carbon-supported Noble Metal Catalysts. *J. Ind. Eng. Chem.* **17**: 287-292 (2011).
10. Luo W, Deka U, Beale AM, Eck ERHv, Bruijnincx PCA, Weckhuysen BM, Ruthenium-catalyzed Hydrogenation of Levulinic Acid: Influence of the Support and Solvent on Catalyst Selectivity and Stability. *J. Catal.* **301**: 175-186 (2013).
11. Mehdi H, Fábos V, Tuba R, Bodor A, Mika LT, Horváth IT, Integration of Homogeneous and Heterogeneous Catalytic Processes for a Multi-step Conversion of

Biomass: From Sucrose to Levulinic Acid, γ-Valerolactone, 1,4-Pentanediol, 2-Methyl-tetrahydrofuran, and Alkanes. *Top. Catal.* **48**: 49-54 (2008).

12. Yan K, Lafleur T, Wu G, Liao J, Ceng C, Xie X, Highly Selective Production of Value-added γ-Valerolactone from Biomass-derived Levulinic Acid using the Robust Pd Nanoparticles. *Appl. Catal. A: Gen.* **468**: 52-58 (2013).
13. Yan Z-P, Lin L, Liu S, Synthesis of γ-Valerolactone by Hydrogenation of Biomass-derived Levulinic Acid over Ru/C Catalyst. *Energy Fuels* **23**: 3853-3858 (2009).
14. Omoruyi U, Page S, Hallett J, Miller PW, Homogeneous Catalyzed Reactions of Levulinic Acid: To γ-Valerolactone and Beyond. *ChemSusChem* **9**: 2037-2047 (2016).
15. Mándity IM, Ötvös SB, Fülöp F, Strategic Application of Residence-time Control in Continuous-flow Reactors. *ChemistryOpen* **4**: 212-223 (2015).
16. Hao Y, Li M, Cárdenas-Lizana F, Keane MA, Selective Production of Benzylamine via Gas Phase Hydrogenation of Benzonitrile over Supported Pd Catalysts. *Catal. Lett.* **146**: 109-116 (2016).
17. Delidovich I, Hausoul PJC, Deng L, Pfützenreuter R, Rose M, Palkovits R, Alternative Monomers Based on Lignocellulose and Their Use for Polymer Production. *Chem. Rev.* **116**: 1540-1599 (2016).
18. Richardson SD and Kimura SY, Water Analysis: Emerging Contaminants and Current Issues. *Anal. Chem.* **88**: 546-582 (2016).
19. Hara M, Nakajima K, Kamata K, Recent Progress in the Development of Solid Catalysts for Biomass Conversion into High Value-added Chemicals. *Sci. Technol. Adv. Mater.* **16**: 034903.1-034903.22 (2015).
20. Ohyama J, Esaki A, Yamamoto Y, Arai S, Satsuma A, Selective Hydrogenation of 2-Hydroxymethyl-5-furfural to 2,5-Bis(hydroxymethyl)furan over Gold Sub-nano Clusters. *RSC Adv.* **3**: 1033-1036 (2013).
21. Wei Z, Li Y, Thushara D, Liu Y, Ren Q, Novel Dehydration of Carbohydrates to 5-Hydroxymethylfurfural Catalyzed by Ir and Au Chlorides in Ionic Liquids. *J. Taiwan Inst. Chem. Eng.* **42**: 363-370 (2011).
22. Budroni G and Corma A, Gold and Gold-platinum as Active and Selective Catalyst for Biomass Conversion: Synthesis of γ-Butyrolactone and One-pot Synthesis of Pyrrolidone. *J. Catal.* **257**: 403-408 (2008).
23. Weingarten R, Tompsett GA, Conner.Jr. WC, Huber GW, Design of Solid Acid

Catalysts for Aqueous-phase Dehydration of Carbohydrates: The Role of Lewis and Brønsted Acid Sites. *J. Catal.* **279**: 174-182 (2011).

24. Ganduglia-Pirovano MV, Hofmann A, Sauer J, Oxygen Vacancies in Transition Metal and Rare Earth Oxides: Current State of Understanding and Remaining Challenges. *Surf. Sci. Rep.* **62**: 219-270 (2007).
25. Mullins DR, The Surface Chemistry of Cerium Oxide. *Surf. Sci. Rep.* **70**: 42-85 (2015).
26. Smith RS, Li Z, Chen L, Dohnálek Z, Kay BD, Adsorption, Desorption, and Displacement Kinetics of H_2O and CO_2 on TiO_2(110). *J. Phys. Chem. B* **118**: 8054-8061 (2014).
27. Farfan-Arribas E and Madix RJ, Role of Defects in the Adsorption of Aliphatic Alcohols on the TiO_2(110) Surface. *J. Phys. Chem. B* **106**: 10680-10692 (2002).
28. Zhou J and Mullins DR, Adsorption and Reaction of Formaldehyde on Thin-film Cerium Oxide. *Surf. Sci.* **600**: 1540-1546 (2006).
29. Sepúlveda-Escribano A, Coloma F, Rodríguez-Reinoso F, Promoting Effect of Ceria on the Gas Phase Hydrogenation of Crotonaldehyde over Platinum Catalysts. *J. Catal.* **178**: 649-657 (1998).
30. Milone C, Ingoglia R, Schipilliti L, Crisafulli C, Neri G, Galvagno S, Selective Hydrogenation of α,β-Unsaturated Ketone to α,β-Unsaturated Alcohol on Gold-supported Iron Oxide Catalysts: Role of the Support. *J. Catal.* **236**: 80-90 (2005).
31. Baker LR, Kennedy G, Spronsen Mv, Hervier A, Cai X, Chen S, Wang L-W, Somorjai GA, Furfuraldehyde Hydrogenation on Titanium Oxide-supported Platinum Nanoparticles Studied by Sum Frequency Generation Vibrational Spectroscopy: Acid–base Catalysis Explains the Molecular Origin of Strong Metal–support Interactions. *J. Am. Chem. Soc.* **134**: 14208-14216 (2012).
32. Paier J, Penschke C, Sauer J, Oxygen Defects and Surface Chemistry of Ceria: Quantum Chemical Studies Compared to Experiment. *Chem. Rev.* **113**: 3949-3985 (2013).
33. Bachiller-Baeza B, Rodríguez-Ramos I, Guerrero-Ruiz A, Influence of Mg and Ce Addition to Ruthenium based Catalysts used in the Selective Hydrogenation of α,β-Unsaturated Aldehydes. *Appl. Catal. A: Gen.* **205**: 227-237 (2001).
34. Khoudiakov M, Gupta MC, Deevi S, Au/Fe_2O_3 Nanocatalysts for CO Oxidation: A Comparative Study of Deposition–precipitation and Coprecipitation Techniques. *Appl.*

Catal. A: Gen. **291**: 151-161 (2005).

35. Lónyi F and Valyon J, On the Interpretation of the NH_3-TPD Patterns of H-ZSM-5 and H-Mordenite. *Micropor. Mesopor. Mater.* **47**: 293-301 (2001).
36. Salasc S, Perrichon V, Primet M, Chevrier M, Mouaddib-Moral N, Oxygen Titration of Spill-over Hydrogen in Ceria and Ceria–alumina Supported Platinum–rhodium Catalysts: Application to the Determination of the Ceria Surface in Contact with Metal. *J. Catal.* **189**: 401-409 (2000).
37. Bond GC, Louis C, Thompson DT, Catalysis by Gold, Imperial College Press, London, 2006.
38. Cárdenas-Lizana F, Wang X, Lamey D, Li M, Keane MA, Kiwi-Minsker L, An Examination of Catalyst Deactivation in Nitroarene Hydrogenation over Supported Gold. *Chem. Eng. J.* **255**: 695-704 (2014).
39. Cárdenas-Lizana F, Gómez-Quero S, Keane MA, Clean Production of Chloroanilines by Selective Gas Phase Hydrogenation Over Supported Ni Catalysts. *Appl. Catal. A: Gen.* **334**: 199-206 (2008).
40. Liu SY and Yang SM, Complete Oxidation of 2-Propanol over Gold-based Catalysts Supported on Metal Oxides. *Appl. Catal. A: Gen.* **334**: 92-99 (2008).
41. Zhang Y, Xiao Q, Bao Y, Zhang Y, Bottle S, Sarina S, Zhaorigetu B, Zhu H, Direct Photocatalytic Conversion of Aldehydes to Esters Using Supported Gold Nanoparticles under Visible Light Irradiation at Room Temperature. *J. Phys. Chem. C* **118**: 19062-19069 (2014).
42. Hao Y, Wang X, Perret N, Cárdenas-Lizana F, Keane MA, Support Effects in the Gas Phase Hydrogenation of Butyronitrile over Palladium. *Catal. Struct. React.* **1**: 4-10 (2015).
43. Costello CK, Guzman J, Yang JH, Wang YM, Kung MC, Gates BC, Kung HH, Activation of Au/γ-Al_2O_3 Catalysts for CO Oxidation: Characterization by X-ray Absorption Near Edge Structure and Temperature Programmed Reduction. *J. Phys. Chem. B* **108**: 12529-12536 (2004).
44. Delannoy L, Weiher N, Tsapatsaris N, Beesley AM, Nchari L, Schroeder SLM, Louis C, Reducibility of Supported Gold (III) Precursors: Influence of the Metal Oxide Support and Consequences for CO Oxidation Activity. *Top. Catal.* **44**: 263-273 (2007).
45. Ousmane M, Liotta LF, Carlo Dd, Pantaleo G, Venezia AM, Deganello G, Retailleau L,

Boreave A, Giroir-Fendler A, Supported Au Catalysts for Low-temperature Abatement of Propene and Toluene, as Model VOCs: Support Effect. *Appl. Catal. B: Environ.* **101**: 629-637 (2011).

46. Hammer B and Nørskov JK, Why Gold is the Noblest of All the Metals. *Nature* **376**: 238-240 (1995).
47. Cárdenas-Lizana F and Keane MA, The Development of Gold Catalysts for Use in Hydrogenation Reactions. *J. Mater. Sci.* **48**: 543-564 (2013).
48. Bus E, Miller JT, Bokhoven JAv, Hydrogen Chemisorption on Al_2O_3-supported Gold Catalysts *J. Phys. Chem. B* **109**: 14581-14587 (2005).
49. Joy NA, Nandasiri MI, Rogers PH, Jiang W, Varga T, Kuchibhatla SVNT, Thevuthasan S, Carpenter MA, Selective Plasmonic Gas Sensing: H_2, NO_2, and CO Spectral Discrimination by a Single Au-CeO_2 Nanocomposite Film. *Anal. Chem.* **84**: 5025-5034 (2012).
50. Ma T-Y, Cao J-L, Shao G-S, Zhang X-J, Yuan Z-Y, Hierarchically Structured Squama-like Cerium-Doped Titania: Synthesis, Photoactivity, and Catalytic CO Oxidation. *J. Phys. Chem. C* **113**: 16658-16667 (2009).
51. Oliveira RL, Bitencourt IG, Passos FB, Partial Oxidation of Methane to Syngas on Rh/Al_2O_3 and Rh/Ce-ZrO_2 Catalysts. *J. Braz. Chem. Soc.* **24**: 68-75 (2013).
52. Radnik J, Mohr C, Claus P, On the Origin of Binding Energy Shifts of Core Levels of Supported Gold Nanoparticles and Dependence of Pretreatment and Material Synthesis. *Phys. Chem. Chem. Phys.* **5**: 172-177 (2003).
53. Campbell CT and Peden CHF, Oxygen Vacancies and Catalysis on Ceria Surfaces. *Science* **309**: 713-714 (2005).
54. Prymak I, Kalevaru VN, Wohlrab S, Martin A, Continuous Synthesis of Diethyl Carbonate from Ethanol and CO_2 over Ce-Zr-O Catalysts. *Catal. Sci. Technol.* **5**: 2322-2331 (2015).
55. Farfan-Arribas E and Madix RJ, Characterization of the Acid−Base Properties of the TiO_2(110) Surface by Adsorption of Amines. *J. Phys. Chem. B* **107**: 3225-3233 (2003).
56. Chupas PJ and Grey CP, Surface Modification of Fluorinated Aluminas: Application of Solid State NMR Spectroscopy to the Study of Acidity and Surface Structure. *J. Catal.* **224**: 69-79 (2004).
57. Jaoude MA, Polychronopoulou K, Hinder SJ, Katsiotis MS, Baker MA, Greish YE,

Alhassan SM, Synthesis and Properties of 1D Sm-doped CeO_2 Composite Nanofibers Fabricated using a Coupled Electrospinning and Sol–gel Methodology. *Ceram. Int.* **42**: 10734-10744 (2016).

58. Morterra C and Magnacca G, A Case Study: Surface Chemistry and Surface Structure of Catalytic Aluminas, As Studied by Vibrational Spectroscopy of Adsorbed Species. *Catal. Today* **27**: 497-532 (1996).
59. Santra C, Pramanik M, Bando KK, Maity S, Chowdhury B, Gold Nanoparticles on Mesoporous Cerium-Tin Mixed Oxide for Aerobic Oxidation of Benzyl Alcohol. *J. Mol. Catal. A: Chem.* **418–419**: 41-53 (2016).
60. Amaniampong PN, Li K, Jia X, Wang B, Borgna A, Yang Y, Titania-Supported Gold Nanoparticles as Efficient Catalysts for the Oxidation of Cellobiose to Organic Acids in Aqueous Medium. *ChemCatChem* **6**: 2105-2114 (2014).
61. Yang M, Men Y, Li S, Chen G, Enhancement of Catalytic Activity over TiO_2-modified Al_2O_3 and $ZnO–Cr_2O_3$ Composite Catalyst for Hydrogen Production via Dimethyl Ether Steam Reforming. *Appl. Catal. A: Gen.* **433-434**: 26-34 (2012).
62. Du X-L, He L, Zhao S, Liu Y-M, Cao Y, He H-Y, Fan K-N, Hydrogen-independent Reductive Transformation of Carbohydrate Biomass into γ-Valerolactone and Pyrrolidone Derivatives with Supported Gold Catalysts. *Angew. Chem.-Int. Edit.* **50**: 7815-7819 (2011).
63. Heeres H, Handana R, Chunai D, Rasrendra CB, Girisuta B, Heeres HJ, Combined Dehydration/(transfer)-hydrogenation of C6-sugars (D-glucose and D-fructose) to γ-valerolactone using Ruthenium catalysts. *Green Chem.* **11**: 1247-1255 (2009).
64. Gao H and Chen J, Hydrogenation of Biomass-derived Levulinic Acid to γ-Valerolactone Catalyzed by PNP-Ir Pincer Complexes: A Computational Study. *J. Organomet. Chem.* **797**: 165-170 (2015).
65. Michel C, Zaffran J, Ruppert AM, Matras-Michalska J, Jędrzejczyk M, Grams J, Sautet P, Role of Water in Metal Catalyst Performance for Ketone Hydrogenation: A Joint Experimental and Theoretical Study on Levulinic Acid Conversion into γ-Valerolactone. *Chem. Commun.* **50**: 12450-12453 (2014).
66. Jain AB and Vaidya PD, Kinetics of the Ruthenium-catalyzed Hydrogenation of Levulinic Acid to γ-Valerolactone in Aqueous Solutions. *Can. J. Chem. Eng.* **94**: 2364-2372 (2016).

67. Kumar VV, Naresh G, Sudhakar M, Anjaneyulu C, Bhargava SK, Tardio J, Reddy VK, Padmasri AH, Venugopal A, An Investigation on the Influence of Support Type for Ni Catalysed Vapour Phase Hydrogenation of Aqueous Levulinic Acid to γ-Valerolactone. *RSC Adv.* **6**: 9872-9879 (2016).
68. Balla P, Perupogu V, Vanama PK, Komandur VRC, Hydrogenation of Biomass-derived Levulinic Acid to γ-Valerolactone over Copper Catalysts Supported on ZrO_2. *J. Chem. Technol. Biotechnol.* **91**: 769-776 (2016).
69. Kumar VV, Naresh G, Sudhakar M, Tardio J, Bhargava SK, Venugopal A, Role of Brønsted and Lewis Acid Sites on Ni/TiO_2 Catalyst for Vapour Phase Hydrogenation of Levulinic Acid: Kinetic and Mechanistic Study. *Appl. Catal. A: Gen.* **505**: 217-223 (2015).
70. Li M, Wang X, Hao Y, Cárdenas-Lizana F, Keane MA, Effect of Support Redox Character on Catalytic Performance in the Gas Phase Hydrogenation of Benzaldehyde and Nitrobenzene over Supported Gold. *Catal. Today* **279**: 19-28 (2017).
71. Calaza FC, Xu Y, Mullins DR, Overbury SH, Oxygen Vacancy-assisted Coupling and Enolization of Acetaldehyde on CeO_2(111). *J. Am. Chem. Soc.* **134**: 18034-18045 (2012).
72. Röbner F, Chapter 5. Elementary Steps and Mechanisms. Section 5.3.2 Spillover Effects in *Handbook of Heterogeneous Catalysis*, ed by G. Ertl HK, F. Schütz, J. Weitkamp. Wiley-VCH, Weinheim,pp 1051-1188 (2008).
73. Manyar HG, Paun C, Pilus R, Rooney DW, Thompson JM, Hardacre C, Highly Selective and Efficient Hydrogenation of Carboxylic Acids to Alcohols using Titania Supported Pt Catalysts. *Chem. Commun.* **46**: 6279-6281 (2010).
74. Hu Q, Yang L, Fan G, Li F, Hydrogenation of Biomass-derived Compounds Containing a Carbonyl Group over a Copper-based Nanocatalyst: Insight into the Origin and Influence of Surface Oxygen Vacancies. *J. Catal.* **340**: 184-195 (2016).
75. Mohan V, Raghavendra C, Pramod CV, Raju BD, Rao KSR, Ni/H-ZSM-5 as a Promising Catalyst for Vapour Phase Hydrogenation of Levulinic Acid at Atmospheric Pressure. *RSC Adv.* **4**: 9660-9668 (2014).
76. Cárdenas-Lizana F, Gómez-Quero S, Keane MA, Ultra-selective Gas Phase Catalytic Hydrogenation of Aromatic Nitro Compounds over Au/Al_2O_3. *Catal. Commun.* **9**: 475-481 (2008).

77. Wang X, Hao Y, Keane MA, Selective Gas Phase Hydrogenation of p-Nitrobenzonitrile to p-Aminobenzonitrile over Zirconia Supported Gold. *Appl. Catal. A: Gen.* **510**: 171-179 (2016).

Table 1. Physico-chemical characteristics of supported Au and Pd catalysts and pseudo-first order rate constant for the transformation of levulinic acid to γ-valerolactone at 493 K (k_{493}).

Catalyst	Au/Al_2O_3	Au/CeO_2	Au/TiO_2	Pd/Al_2O_3
SSA ($m^2\ g^{-1}$)	166	108	52	156
TPR H_2 consumption × 10^2 (μmol g^{-1})	1[a]/1[b]	5[a]/2[b]	2[a]/1[b]	-
H_2 chemisorption (μmol g^{-1})[c]	5	3	4	17
O_2 chemisorption × 10^{-2} (μmol m^{-2})[c]	1	21	23	2
d (nm)	4.3	3.0	3.2	3.0
(NH_3 chemisorption[d] / TPD) × 10^{-2} (mmol g^{-1})	15/16	23/28	12/12	-
k_{493} (h^{-1})	33	83	96	128

[a]experimentally determined value
[b]theoretical value for $Au^{3+} \rightarrow Au^0$
[c]titration at 493K
[d]titration at 298K

Figure Captions

Figure 1: Reaction pathways involved in the transformation of levulinic acid (LA) to the target (framed) γ-valerolactone (GVL).

Figure 2: (I) TPR and **(II)** NH_3-TPD profiles for **(A)** Au/Al_2O_3, **(B)** Au/CeO_2 and **(C)** Au/TiO_2.

Figure 3: Representative **(I)** STEM images and **(II)** associated Au particle size distributions for **(A)** Au/Al_2O_3, **(B)** Au/CeO_2 and **(C)** Au/TiO_2.

Figure 4: Variation of γ-valerolactone selectivity (S_{GVL}) with **(I)** levulinic acid (LA) fractional conversion (X) under reaction conditions in excess of hydrogen (H_2/LA = 420) and **(II)** inlet H_2/LA at full LA conversion (X = 1) over Au/Al_2O_3 (○), Au/CeO_2 (△) and Au/TiO_2 (◇); *Reaction Conditions*: T = 493-573 K, P = 1 atm, $n/F = 5 \times 10^{-4} - 1 \times 10^{-2}$ h.

Figure 5: (I) Pseudo-first order kinetic plot for the conversion of levulinic acid (LA) to γ-valerolactone (GVL) over Au/Al_2O_3 (○), Au/CeO_2 (△) and Au/TiO_2 (◇) with **(II)** Arrhenius plot for reaction over Au/Al_2O_3; *Reaction Conditions*: T = 493-573 K, P = 1 atm, H_2/LA = 420.

Figure 1

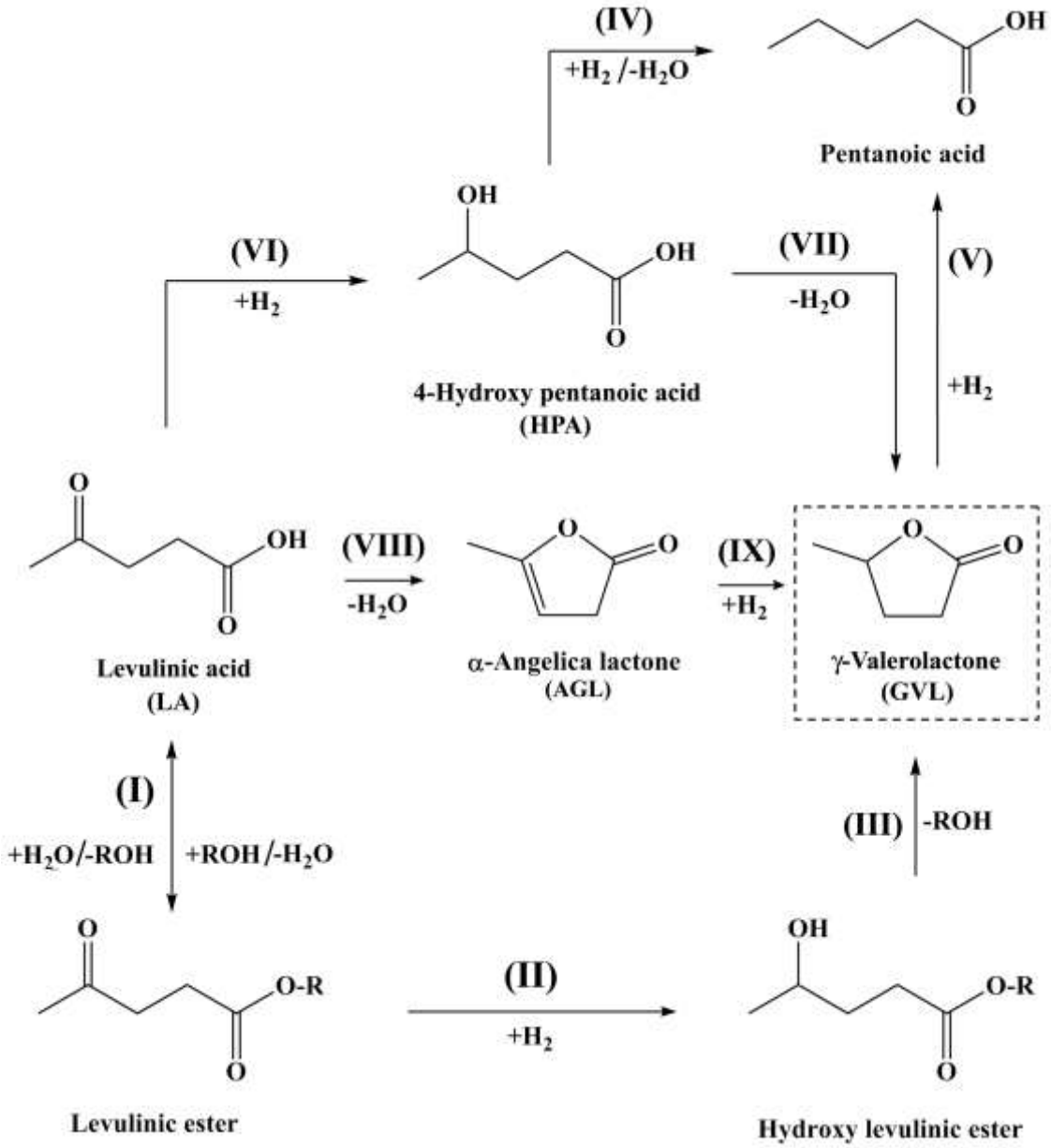
(IV)
+H2 /-H2O
OH
O
Pentanoic acid
OH
(VI)
+H2
OH
O
(VII)
-H2O
(V)
+H2
4-Hydroxy pentanoic acid
(HPA)
O
OH
O
(VIII)
-H2O
O
O
(IX)
+H2
O
O
Levulinic acid
(LA)
α-Angelica lactone
(AGL)
γ-Valerolactone
(GVL)
(I)
+H2O/-ROH
+ROH/-H2O
(III)
-ROH
O
O-R
O
(II)
+H2
OH
O-R
O
Levulinic ester
Hydroxy levulinic ester

Figure 2

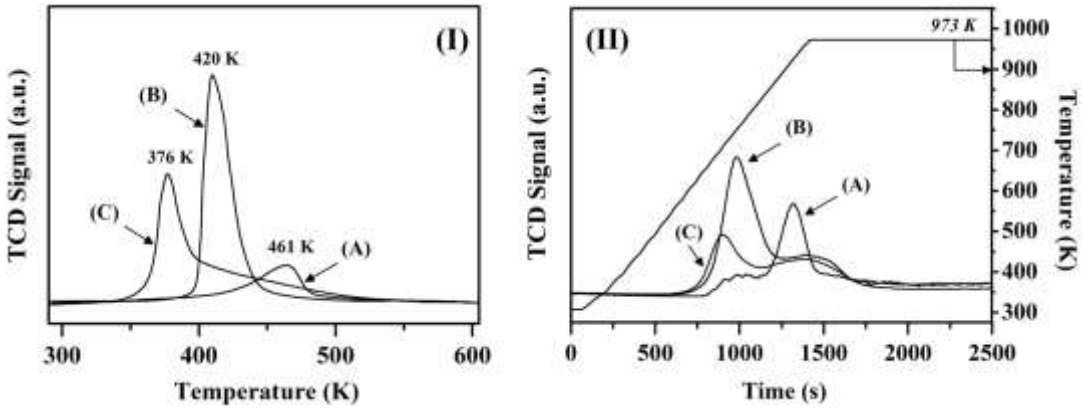
(I)
420 K
(B)
376 K
(C)
461 K
(A)
TCD Signal (a.u.)
300
400
500
600
Temperature (K)
(II)
973 K
(B)
(A)
(C)
TCD Signal (a.u.)
0
500
1000
1500
2000
2500
Time (s)
1000
900
800
700
600
500
400
300
Temperature (K)

Figure 3

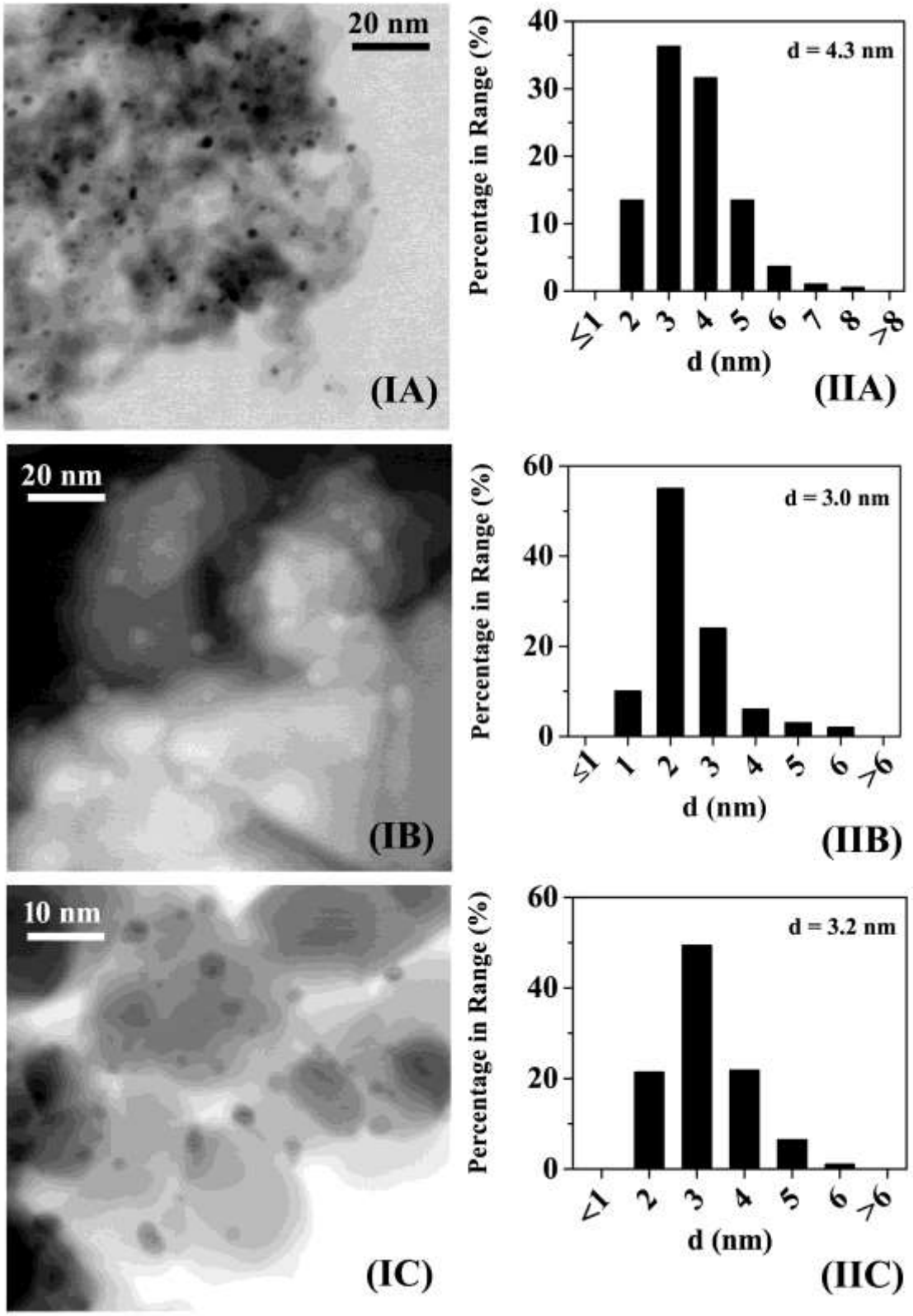
20 nm
(IA)
Percentage in Range (%)
d = 4.3 nm
d (nm)
(IIA)
20 nm
(IB)
d = 3.0 nm
(IIB)
10 nm
(IC)
d = 3.2 nm
(IIC)

Figure 4

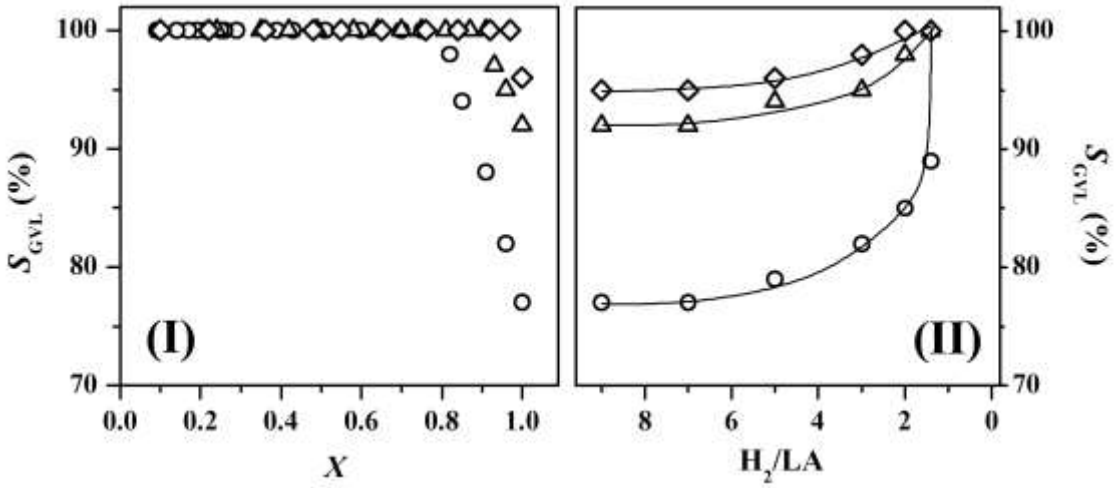

Figure 5